Research Article | Vol. 30, No. 24 / 21 Nov 2022 / Optics Express 43293
Optics EXPRESS

# Multi-pixel photoconductive emitters for the controllable generation of azimuthal and radial terahertz beams

JUSTAS DEVEIKIS AND JAMES LLOYD-HUGHES*

*University of Warwick, Department of Physics, Gibbet Hill Road, Coventry, CV4 7AL, United Kingdom*
**j.lloyd-hughes@warwick.ac.uk*

**Abstract:** A multi-pixel photoconductive emitter is reported that generates THz beams with either azimuthal, radial or linear polarization states. Switching between the different polarization states was purely electrical, via the bias voltage applied, circumventing the need for mechanical polarization optics or different THz emitters to change the polarization. Dipole array modelling was performed to validate emitter array designs, and to explore their optimal bias configuration, while spatially-resolved electro-optic detection of the generated beams confirmed that cylindrical-vector beams were produced. We further demonstrate that the spatial beam profile was optimized by adjusting the bias level on particular pixels, improving the polarization purity of the beam.



## 1. Introduction

Due to their inhomogeneous polarization states, cylindrical-vector (CV) beams have properties distinct from those of Gaussian beams, which have uniform polarization. The fascinating features of azimuthal and radial CV beams under tight focusing conditions have been well reported and include: enhanced longitudinal electric or magnetic fields with respect to the transverse component [1], smaller spot sizes for focused beams than for linearly-polarized beams [2] and extremely long focal depths [3]. These special features are of interest in applications that include optical tweezers for trapping particles [4,5], image resolution improvement in microscopy [6,7] and particle acceleration [8].

The demand for laser-driven terahertz (THz) sources has increased over the last decade and photoconductive interdigitated emitters [9] are attractive sources of pulsed broadband THz radiation. The generation of azimuthal and radial THz beams has been explored, for instance with an interdigitated electrode geometry [10–12], or with a single pair of contacts [13], where the azimuthal or radial acceleration of charge carriers in the semiconductor substrate generated the respective CV modes. Alternative methods reported to produce azimuthal and radial THz beams without employing photoconductive emitters include: optical rectification via velocity-mismatch [14], air-plasma filaments [15], density modulated plasmas [16], segmented [111]-orientation GaP crystals [17] and a spintronic THz emitter used in conjunction with a triangular Si prism [18]. Radially-polarized THz beams can also be converted into vortex beams carrying orbital angular momentum [19].

Full control of the THz beam polarization state may be useful for novel spectroscopy experiments, THz communications, THz polarization imaging [20], and for THz ellipsometry systems. It has been recently shown that multi-pixel photoconductive emitters enable the precise electrical control of the polarization angle of broadband linearly-polarized THz beams [21], while integrating a multi-pixel emitter with an achromatic waveplate allowed the broadband ellipticity to be smoothly and precisely changed from linear to circular [22]. In methods reported previously for the generation of azimuthal and radial THz beams, the experimental setup had to be

#473086 https://doi.org/10.1364/OE.473086
Journal © 2022 Received 11 Aug 2022; revised 7 Sep 2022; accepted 7 Sep 2022; published 9 Nov 2022

Optics EXPRESS

rearranged to support the production of the desired polarization state (e.g. swapping one emitter for another), requiring careful and time-consuming re-alignment procedures, and introducing system complexity.

In this Article, we illustrate full THz polarization control between linearly-, azimuthally- and radially-polarized THz beams with one compact component, a multi-pixel photoconductive array. A rapid and convenient switching between polarization states was achieved by using different electrical bias configurations on the pixels. Dipole array simulations were used to predict the performance of the device geometry, which consisted of 16 active pixels. To validate the generation of the desired CV beam, we determined the beam's polarization state profile using spatially-resolved electro-optic sampling. Finally, we introduce the ability to electrically modify and improve the CV beam quality in a controlled manner.

## 2. Experimental methods and modelling

Interdigitated photoconductive emitters are made of metal electrodes on the surface of semiconductor, forming a periodic structure of cathode, semiconductor gap and anode [9,23]. A fs pulse is used to irradiate semiconductor, which excites charge carriers in the biased semiconductor region only. Accelerated charge carriers create transient photocurrents that radiate THz pulses, while the pulse from each excited semiconductor area can interfere constructively in the far-field. Interdigitated emitters were used in this work due to their improved polarization purity and good radiation pattern in comparison to bow-tie or narrow-gap strip line antennae [24].

The interdigitated emitter used in this study was fabricated employing laser-write photolithography, with metal deposition by a magnetron sputtering, on a 500 $\mu$m thickness semi-insulating GaAs substrate. The emitter was made of 16 pixels, each with an area 100×100 $\mu$m$^2$ and metal electrodes that were 5 $\mu$m wide, with 5 $\mu$m gaps, as displayed in Fig. 1 (a). Adjacent pixels were designed to generate orthogonally polarized THz beams (horizontally and vertically) and the direction of the bias electric field determined the polarity of the radiated THz pulse. The electrical bias used square waves at 100 kHz frequency, with 10 V amplitude and 50% duty cycle. The THz radiation emitted by each pixel interfered constructively in the far-field to produce a coherent THz beam. Using 16 pixels allowed control of the local polarization state, with enhanced polarization purity and quality of azimuthal and radial THz beam in comparison to designs with a 9 pixels (3x3 configuration). A custom THz time-domain spectrometer was used in this work, based on a Ti:Sapphire oscillator with a 70 fs pulse duration. An average power of 700 mW was used to excite the emitter, with a beam size selected to uniformly cover the ~600×600 $\mu$m$^2$ active area.

### 2.1. Dipole array modelling

The THz radiation pattern produced from the multi-pixel array was calculated by approximating the THz radiation emitted from the active semiconductor areas using an array of electrical dipoles that matched the emitter geometry. The typical wavelength of 300 $\mu$m (1 THz) is much smaller than the dipole size (5 $\mu$m), hence the Hertzian dipole approximation was used to calculate the vector electric field of each dipole. The electric field components produced by a Hertzian dipole in a spherical coordinate system $r$, $\theta$ and $\rho$ are

$$E_r = Z_0 \frac{I_0 l \cos\theta}{2\pi r^2}\left(1 + \frac{1}{ikr}\right)e^{-ikr}, \tag{1}$$

$$E_\theta = iZ_0 \frac{kI_0 l \sin\theta}{4\pi r}\left(1 + \frac{1}{ikr} - \frac{1}{(kr)^2}\right)e^{-ikr}, \tag{2}$$

$$E_\phi = 0, \tag{3}$$

where $l$ is the length of dipole, $Z_0$ is the impedance of free space, $I_0$ is the photocurrent, $k$ is the wavenumber, $i$ is the imaginary unit. The parameters of the model were selected to match typical

Optics EXPRESS

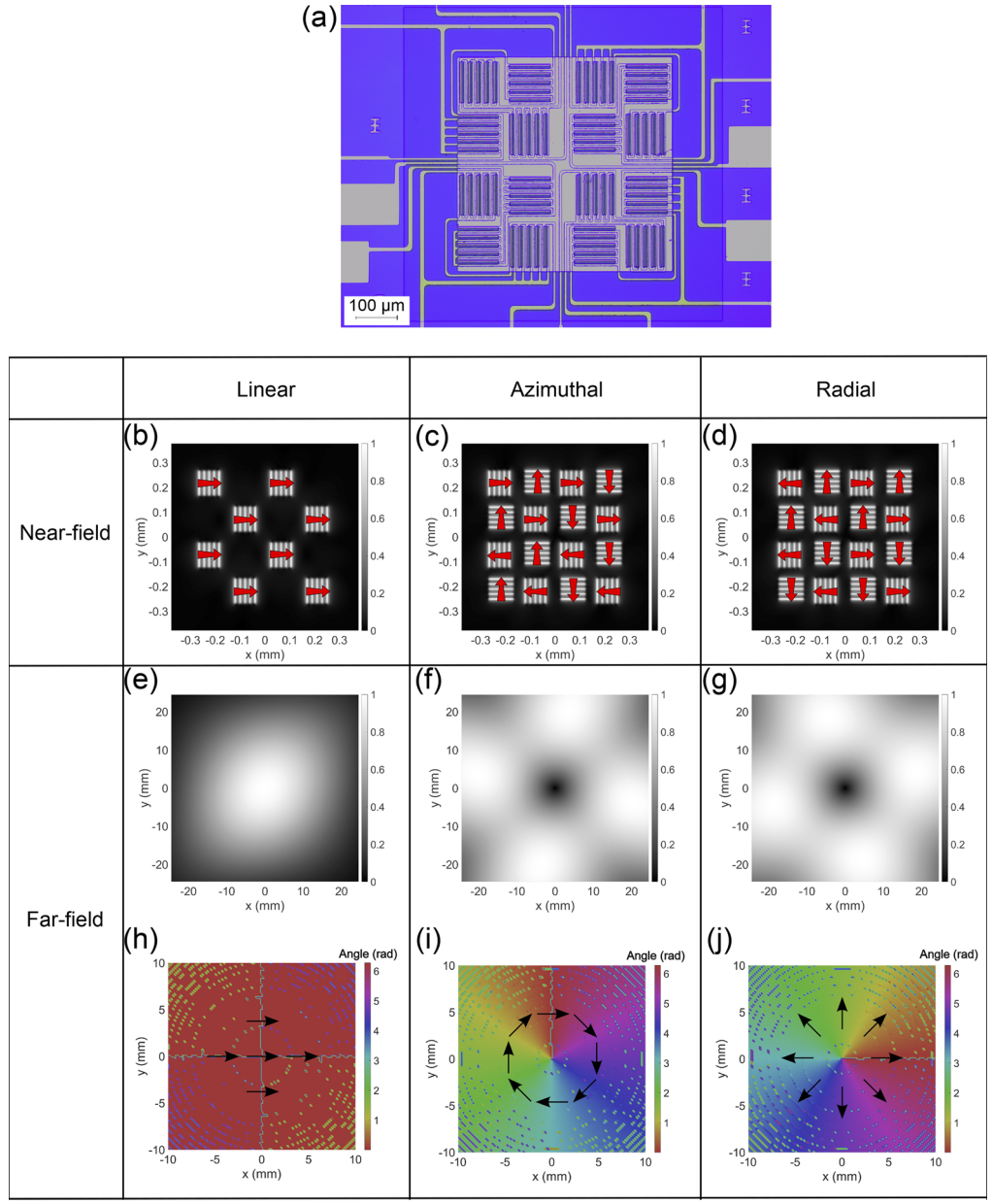


**Fig. 1.** (a) Optical microscopy images of 16-pixel interdigitated emitter active area. (b), (c), (d) Spatial transverse electric field distribution in the near-field (5 $\mu$m) and (e), (f), (g) in the far-field (50 mm) and ; (h), (i), (j) color maps displaying the orientation of local electric field in the far-field for linearly, azimuthally and radially polarized beam respectively. Red arrows are parallel to the direction of bias electric field in the semiconductor gaps.

interdigitated photoconductive devices: for instance the orientation and position of dipoles was created to match the geometry of exposed semiconductor gaps in the device. Each dipole had a length of 5 $\mu$m and the distance between adjacent dipoles in the same semiconductor gap was 5 $\mu$m.

Optics EXPRESS

The modelling results of transverse electric field amplitude and orientation in the near- and far-field at 1 THz are presented in Fig. 1. The modelled data show that different biasing conditions of the same 16-pixel emitter result in different polarization states in the far-field. Panels (b)-(d) present the THz intensity in the $x-y$ plane in the near-field while (e)-(g) show the far-field intensity and (h)-(j) the far-field polarization angle distribution for horizontally-, azimuthally- and radially-polarized beams. The modelling results show that when configured to generate a linearly-polarized THz beam the emitter produces a Gaussian beam profile and a uniform polarization state in the $x-y$-plane. The CV beams possess a doughnut-like intensity profile and a cyclic polarization angle distribution, in good agreement with expectations for CV beams [6,25]. It is worth noting that the beam profiles of the azimuthal and radial beams are not perfect because of the finite number of pixels used and their square shape: further improvements could be made, for instance using designs with a larger number of smaller pixels.

### 2.2. Spatially-resolved electro-optic sampling

Due to their non-Gaussian beam profile and polarization inhomogeneity, we adopted spatially-resolved electro-optic sampling (SR-EOS) to sample the vectoral THz electric field at different spatial positions. This method involved scanning the probe beam with respect to the THz beam at the electro-optic crystal, which was a 2 mm thick $\langle 110 \rangle$ - oriented ZnTe crystal. A similar approach has already been used by introducing additional delay stage with two mirrors [8] or expanding the probe beam and moving iris across [17]. In this study, the probe beam was expanded in horizontal direction using a pair of convex cylindrical lenses, as shown in Fig. 2 (a), to beam widths of 1.5 mm×0.45 mm horizontally and vertically (values indicate D4$\sigma$). Probe beam profiles and positions were monitored with a custom-built beam profiler based on a Raspberry Pi HQ camera, similar to Ref. [26]. The slit width was adjusted to 600 $\mu$m, and was placed on a mechanical stage to allow the ready alteration of the position of the probe beam on the detection crystal. A spherical lens was used to further reduce the gate beam size at the crystal to 280 $\mu$m ×450 $\mu$m, smaller than the THz beam size at the detection crystal, which was approximately 1.4 mm×1.4 mm. The electro-optic signal is proportional to the product of THz electric field strength and the optical power of the probe beam [20], but the incident optical power of the gate beam changed slightly as the slit was scanned across the probe beam. To account for this, the electro-optic signal was normalized by the gate beam power transmitted through the electro-optic crystal at different slit positions. The horizontal and vertical components of the THz electric field were resolved by rotating the detection crystal and gate beam polarization.

Experimental results from SR-EOS applied to the multi-pixel emitter are reported in Fig. 2 under the bias conditions required to produce azimuthal or radial CV beams. Panel (b) illustrates the transverse electric field profile of an azimuthally-polarized beam, while panel (c) indicates the THz electric field sampled at the peak of the time-domain pulse. A strong vertical component is evident, which swaps sign across the beam centre near zero probe beam position. Further information can be seen in contour maps of the vertical component of the THz pulse as a function of EOS time and probe beam position (Fig. 2(d)). In particular, the top/bottom mirror symmetry about zero probe beam position indicates that the time-domain THz pulse had a similar shape and duration for all positions off the axis. The symmetry was consistent at different EOS times confirming that the THz pulses produced were broadband and with a fixed phase relation. Results obtained when the multi-pixel emitter was biased to produce radial polarization, as pictured in Fig. 2 (e), are reported in panels (f) and (g). A strong horizontal component can be seen, which also changed sign across the beam centre. These results agree with expectations from CV beam theory and previous studies of azimuthally- or radially-polarized THz beams [11,17].

Optics EXPRESS

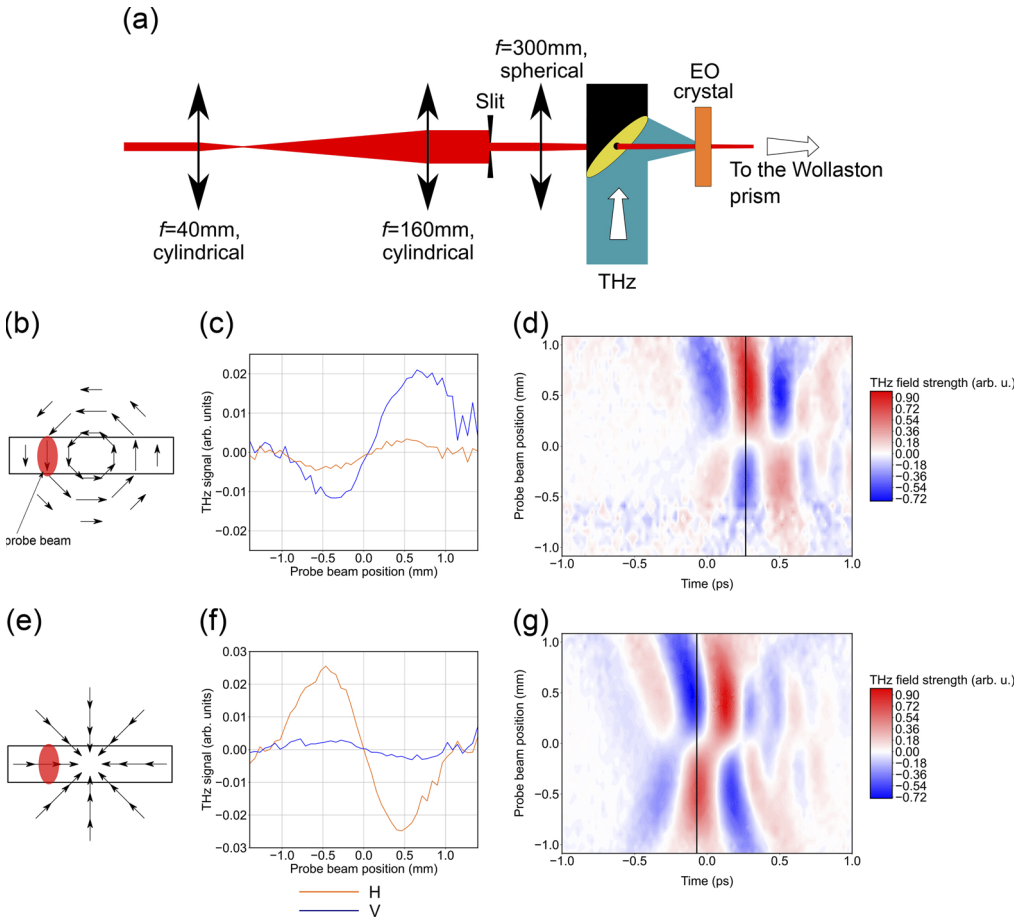


**Fig. 2.** (a) Diagram of the spatially-resolved electro-optic sampling setup used (top-down view). (b) Schematic spatial profile of the transverse electric field for an azimuthal beam (arrows). The black rectangle shows the approximate extent of gate beam positions probed. (c) Beam profile measurements by aperture scanning of vertical (blue) and horizontal (orange) electric field components for the azimuthal beam, obtained at the time-delay indicated by a vertical black line in (d). (d) Time-domain THz pulses at different aperture positions. (e)-(g) are as (b)-(d), but for a radial THz beam.

### 2.3. *Optimising the polarization state*

Since the bias voltage on each pixel can be controlled independently, the CV beam profile may be fine-tuned to improve the quality and symmetry of the beam towards the theoretical profile, as will now be discussed for the example of radially-polarized THz beams. The lowest order radial CV beam can be described as the product of a Gaussian and a Bessel function, yielding a function that is odd in probe beam position, $x$ [27]:

$$E_x \propto J_1(x) e^{-(x-x_0)^2/2\sigma^2}, \tag{4}$$

where $E_x$ is the horizontal component of the THz electric field; $J_1(x)$ is the Bessel function of the first kind of order one; $x_0$ and $\sigma$ are the central position and standard deviation of the Gaussian used to fit the data. The experimental optimisation of the radial beam profile is reported in Fig. 3. A SR-EOS measurement of the horizontal THz field component was performed with all pixels

Optics EXPRESS

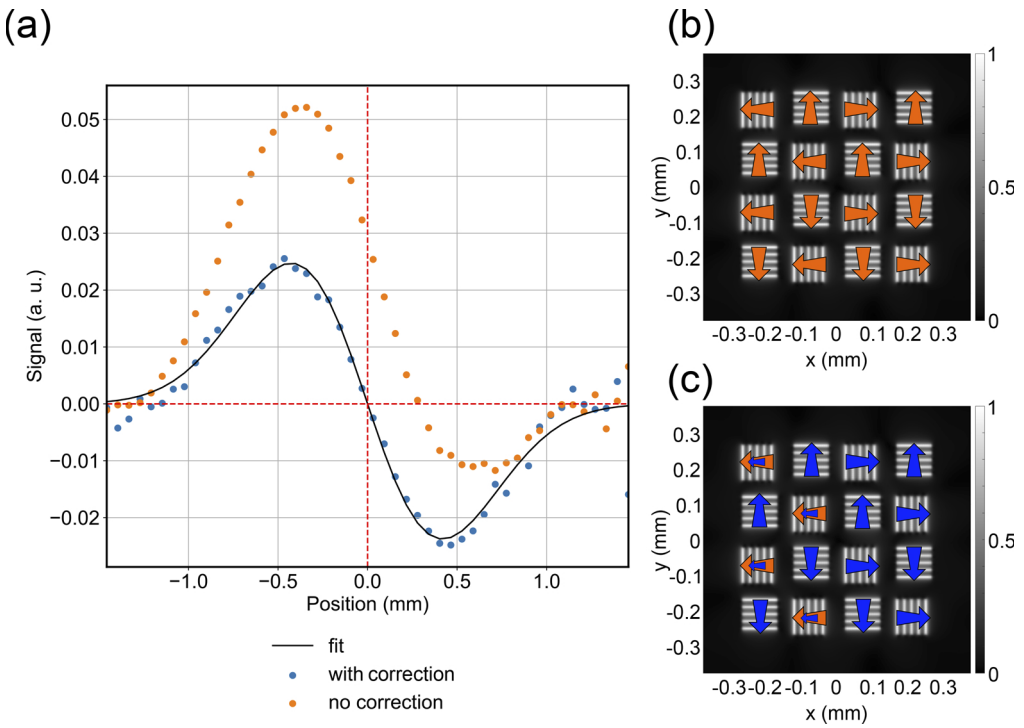


**Fig. 3.** Electrical control of the radial THz beam profile. (a) Normalized radial beam profile obtained by using 10 V bias voltage on each pixel (orange points) and with an adjusted bias voltage pattern (blue points). The theoretical profile for a radial beam (black curve) is also shown. (b) and (c) show the bias voltage configurations used to produce two different beam profiles given in (a); arrows are parallel to the electric field direction and their length is proportional to the amplitude of electric field.

driven by square wave of 10 V amplitude, as pictured in Fig. 3 (b), but this configuration resulted in the distorted and asymmetric beam profile in Fig. 3 (a) (orange points), with greater THz electric field for $x<0$ than for $x>0$. This may have resulted from small alignment errors, such as slightly more pump power on one side of the emitter than the other. An improved beam shape was achieved by attenuating the voltage on specific pixels to 7 V (illustrated in Fig. 3 (c)), making the beam more symmetric (blue points). The corrected beam profile is in excellent agreement with the theoretical profile of Eq. (4), reported by the solid black line in Fig. 3 (a).

## 3. Conclusions

Dipole array calculations were used to evaluate the electric field distribution of azimuthally- and radially-polarized THz beams produced by a 16-pixel emitter under different biasing conditions. A 16-pixel emitter was successfully used to generate linear, azimuthal and radial THz beams and a SR-EOS method was employed to measure the profiles of the CV beams. Unique features of CV beams were observed: a sign inversion of the THz pulse as the probe beam was scanned across the beam centre, and a zero transverse electric field at the centre of the beam. The ability to control the beam profile and polarization state was demonstrated without any need for mechanical realignment of the emitter, and in a way that could correct for optical alignment errors.

Future work could involve analysis on how changing the number, positioning, shape and size of the pixels impacts on the generated THz beam, with a view to further optimising beam parameters and polarization purity. It would be useful to map the polarization state across the entire plane of

Optics EXPRESS

the beam, allowing more detailed analysis of CV beams. This approach could be implemented by using an aperture and an additional mechanical stage to enable movement of the aperture in two orthogonal directions, or by using a THz camera and a pair of polarizers to image different polarization components of electric field. Finally, the controlled production of CV beams via the multi-pixel concept allows the rapid switching between vortex beams with different topological charge.

**Funding.** Engineering and Physical Sciences Research Council (EP/V047914/1).

**Acknowledgments.** The authors thank D. Greenshields for creating the 16-channel voltage driver used in this work.

**Disclosures.** The authors declare no conflicts of interest.

**Data availability.** Data underlying the results presented in this paper are not publicly available at this time but may be obtained from the authors upon reasonable request.

## References

1. H. P. Urbach and S. F. Pereira, "Field in focus with a maximum longitudinal electric component," Phys. Rev. Lett. **100**(12), 123904 (2008).
2. R. Dorn, S. Quabis, and G. Leuchs, "Sharper focus for a radially polarized light beam," Phys. Rev. Lett. **91**(23), 233901 (2003).
3. H. Wang, L. Shi, B. Lukýanchuk, C. Sheppard, and C. T. Chong, "Creation of a needle of longitudinally polarized light in vacuum using binary optics," Nat. Photonics **2**(8), 501–505 (2008).
4. Q. Zhan, "Trapping metallic Rayleigh particles with radial polarization," Opt. Express **12**(15), 3377–3382 (2004).
5. S. E. Skelton, M. Sergides, R. Saija, M. A. Iatì, O. M. Maragó, and P. H. Jones, "Trapping volume control in optical tweezers using cylindrical vector beams," Opt. Lett. **38**(1), 28–30 (2013).
6. K. S. Youngworth and T. G. Brown, "Focusing of high numerical aperture cylindrical-vector beams," Opt. Express **7**(2), 77–87 (2000).
7. D. P. Biss, K. S. Youngworth, and T. G. Brown, "Dark-field imaging with cylindrical-vector beams," Appl. Opt. **45**(3), 470–479 (2006).
8. M. J. Cliffe, A. Rodak, D. M. Graham, and S. P. Jamison, "Generation of longitudinally polarized terahertz pulses with field amplitudes exceeding 2kv /cm," Appl. Phys. Lett. **105**(19), 191112 (2014).
9. A. Dreyhaupt, S. Winnerl, T. Dekorsy, and M. Helm, "High-intensity terahertz radiation from a microstructured large-area photoconductor," Appl. Phys. Lett. **86**(12), 121114 (2005).
10. B. Zimmermann, F. Peter, H. Schneider, M. Helm, and S. Winnerl, "Terahertz Bessel-Gauss beams of radial and azimuthal polarization from microstructured photoconductive antennas," Opt. Express **17**(3), 1571–1576 (2009).
11. S. Winnerl, R. Hubrich, M. Mittendorff, H. Schneider, and M. Helm, "Universal phase relation between longitudinal and transverse fields observed in focused terahertz beams," New J. Phys. **14**(10), 103049 (2012).
12. K. Kan, J. Yang, A. Ogata, S. Sakakihara, T. Kondoh, K. Norizawa, I. Nozawa, T. Toigawa, Y. Yoshida, H. Kitahara, K. Takano, M. Hangyo, R. Kuroda, and H. Toyokawa, "Radially polarized terahertz waves from a photoconductive antenna with microstructures," Appl. Phys. Lett. **102**(22), 221118 (2013).
13. S. Waselikowski, C. Fischer, J. Wallauer, and M. Walther, "Optimal plasmonic focusing on a metal disc under radially polarized terahertz illumination," New J. Phys. **15**(7), 075005 (2013).
14. A. Galvanauskas, C. J. Divin, C.-H. Liu, G. Chang, S. L. Williamson, and T. B. Norris, "Generation of radially polarized terahertz pulses via velocity-mismatched optical rectification," Opt. Lett. **32**(4), 433–435 (2007).
15. Y. Minami, T. Kurihara, K. Yamaguchi, M. Nakajima, and T. Suemoto, "Longitudinal terahertz wave generation from an air plasma filament induced by a femtosecond laser," Appl. Phys. Lett. **102**(15), 151106 (2013).
16. S. Chaudhary Manendra, K. P. Singh, U. Verma, and A. K. Malik, "Radially polarized terahertz (THz) generation by frequency difference of hermite cosh gaussian lasers in hot electron-collisional plasma," Opt. Lasers Eng. **134**, 106257 (2020).
17. K. Konishi, M. Kuwata-Gonokami, N. Kanda, R. Imai, T. Higuchi, and Z. Zheng, "Terahertz vector beam generation using segmented nonlinear optical crystals with threefold rotational symmetry," Opt. Express **20**(20), 21896–21904 (2012).
18. H. Niwa, N. Yoshikawa, M. Kawaguchi, M. Hayashi, R. Shimano, and R. Shimano, "Switchable generation of azimuthally- and radially-polarized terahertz beams from a spintronic terahertz emitter," Opt. Express **29**(9), 13331–13343 (2021).
19. K. Konishi, M. Kuwata-Gonokami, N. Kanda, R. Imai, and T. Higuchi, "Generation of broadband terahertz vortex beams," Opt. Lett. **39**(13), 3714–3717 (2014).
20. N. C. J. van der Valk, W. A. M. van der Marel, and P. C. M. Planken, "Terahertz polarization imaging," Opt. Lett. **30**(20), 2802–2804 (2005).
21. C. D. Mosley, M. Staniforth, A. I. Serrano, E. Pickwell-Macpherson, and J. Lloyd-Hughes, "Scalable interdigitated photoconductive emitters for the electrical modulation of terahertz beams with arbitrary linear polarization," AIP Adv. **9**(4), 045323 (2019).

Optics EXPRESS

22. C. D. Mosley, J. Deveikis, and J. Lloyd-Hughes, "Precise and accurate control of the ellipticity of THz radiation using a photoconductive pixel array," Appl. Phys. Lett. **119**(12), 121105 (2021).
23. A. Singh, H. Schneider, M. Welsch, M. Helm, and S. Winnerl, "Improved electrode design for interdigitated large-area photoconductive terahertz emitters," Opt. Express **27**(9), 13108–13115 (2019).
24. C. D. Mosley, M. Failla, D. Prabhakaran, and J. Lloyd-Hughes, "Terahertz spectroscopy of anisotropic materials using beams with rotatable polarization," Sci. Rep. **7**, 12337–12338 (2017).
25. Q. Zhan, "Cylindrical vector beams: from mathematical concepts to applications," Adv. Opt. Photonics **1**(1), 1–57 (2009).
26. J. Keaveney, "Automated translating beam profiler for in situ laser beam spot-size and focal position measurements," Rev. Sci. Instrum. **89**(3), 035114 (2018).
27. D. G. Hall, "Vector-beam solutions of Maxwell's wave equation," Opt. Lett. **21**(1), 9–11 (1996).